EXPERIMENT 03

FABRY PEROT RESONATOR
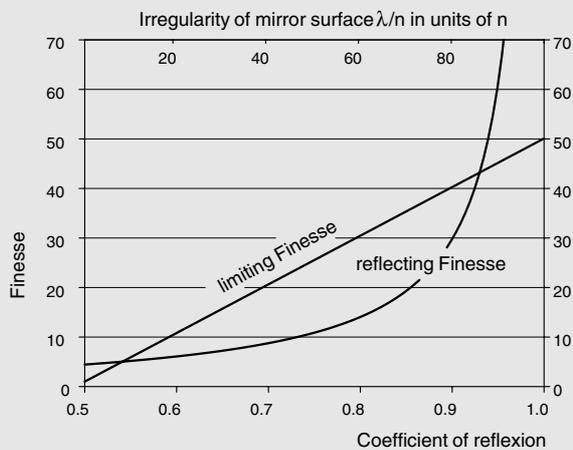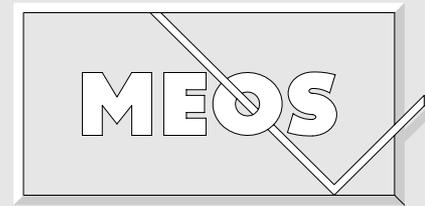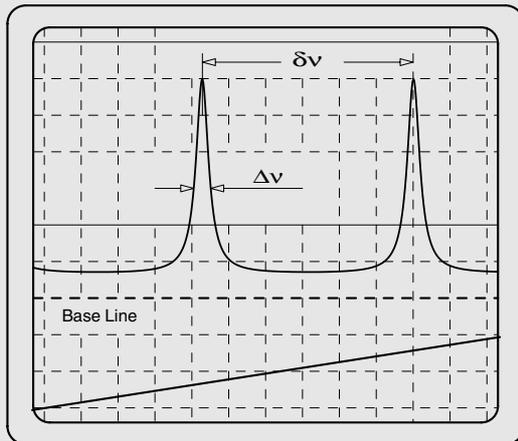
Didactic Counsellor

Prof. Dr.-Ing. Dickmann
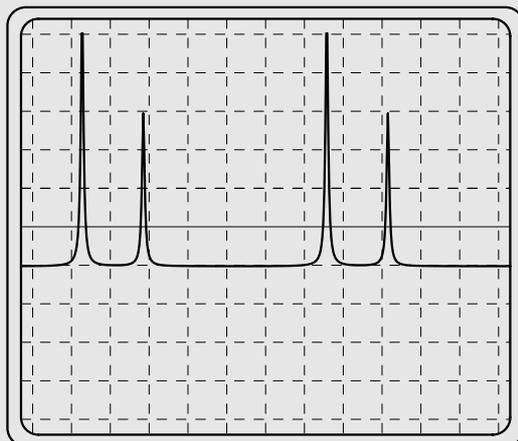
Fachhochschule Münster

Fachbereich Physikal. Technik

1 Fundamentals

Fabry Perot resonators function not only as indispensable parts of lasers but also as high-resolution optical spectrum analysers. This means the functioning is based on the superposition or interference of light. Jamin (J. Jamin, Pogg. Ann., Vol.98 (1856) P.345) first built an interference device in 1856. He could measure the relative refractive index of optical media accurately with this device (Fig. 1).
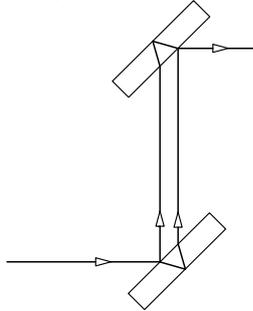
Fig. 1: Jamin's interferometer - 1856

This formed the basis on which Mach and Zehnder developed an interferometer of great significance in 1892 (E. Mach Z. - Building instruments, Vol.12 (1892), P.89), now known as the Mach-Zehnder interferometer (Fig. 2). It has become very important in laser measuring techniques. e.g. this type of interferometer is used for laser vibrometers.
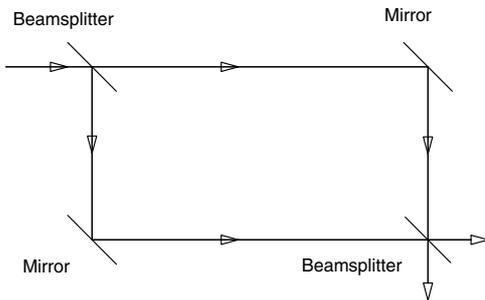
Fig. 2: Mach-Zehnder interferometer.

The most well-known interferometer however, was developed by Michelson in 1882 (A. A. Michelson, Philos. Mag.(5) Vol.13 (1882) P.236). The following explanation of light interference uses this type of interferometer as an example.
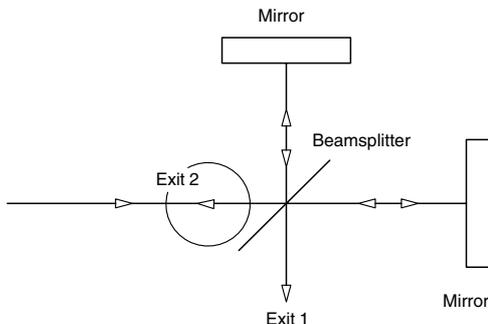
Fig. 3: Michelson interferometer
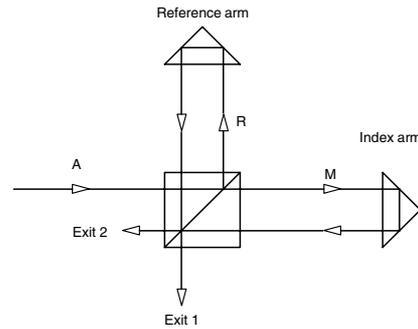
Fig. 4: Modern technical Michelson interferometer for interferometrical measurement of length by laser

A laser beam A hits the beam-splitting prism as shown in Fig. 4. At this point it is split up into the two components R (reference beam) and M (measuring beam). This is an important characteristic of this type of interferometer. They are therefore called two-beam interferometers, whereas in the interferometers or resonators developed later by Fabry Perot, not just two, but many beams were made to interfere. This type of interferometer is therefore known as a multi-beam interferometer (Fig. 5).

In this interferometer constructed by A. Fabry and Ch. Perot (1897) the incoming light beam is split into many individual components which all interfere with each other.
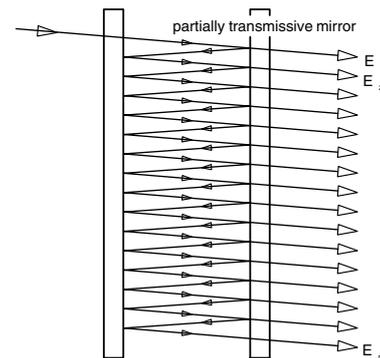
Fig. 5: The multibeam interferometer by A. Fabry and Ch. Perot, 1897, is still used today in high-resolution spectroscopy and as a laser resonator (but, mainly with curved mirrors).

To understand the Fabry Perot we should first examine the interference of two beams and then calculate the interference for many beams.

1.1 Two beam interference

Let us first look at the Michelson Interferometer as shown in Fig. 4 once more. The incoming light beam has an electric field E_A which oscillates at a frequency ω and has travelled the path r_A.

$$E_A = A_0 \cdot \sin\left(\omega t + k r_A\right)$$

A_0 is the maximum amplitude and k is the wave number

$$k = \frac{2\pi}{\lambda}.$$

The result for the field E_R is:

$$E_R = A_R \cdot \sin(\omega t + k x_R + \varphi_R)$$

and for the field E_M:

$$E_M = A_M \cdot \sin(\omega t + k x_M + \varphi_R)$$

$k(x_R\text{-}x_M)$ is the phase shifting of the measurement wave as opposed to the reference wave, which occurs because the path of the measuring beam through the index arm of the interferometer is longer or shorter than the path of the reference arm. This phase shifting is also known as the path difference and is symbolised as δ.

φ_R and φ_M are phase changes occurring through reflection at a boundary surface. When reflection occurs on an ideal reflector, a phase shift of 180° takes place.

If we follow the path of the measuring beam up to Exit 1, we can see that the reference beam goes through two reflections and the measuring beam goes through three reflections. The measuring beam undergoes a phase shift of 180° as opposed to the reference beam. The shift in field intensity of 180° is marked with an *. From the point within the beam-splitter, as shown in Fig. 4, where the measuring and reference beams meet, the field intensities add up at Exit 1 to E_1 and/or at *Exit 2* to E_2, resulting in:

$$E_1 = E_2 + E_M^* \qquad\qquad E_2 = E_R^* + E_M$$

$$E_1 = A_R \sin(\omega t + k x_R) - A_M \sin(\omega t + k x_M)$$

$$E_2 = -A_R \sin(\omega t + k x_R) + A_M \sin(\omega t + k x_M)$$

because: $\sin(\alpha + 180) = \sin(\alpha)$.

However, field intensity cannot be measured on the spot, so the luminous intensity I, which is a result of the square of the electrical field strength of the light, has to be perceived by the eye or by using a photo detector:

$$I = E_{light}^2$$

Therefore for Exit 1:

$$I_1 = \left(A_R \sin(\omega t + k x_R) - A_M \sin(\omega t + k x_M) \right)^2$$

A short calculation shows this result:

$$\begin{aligned} I_1 = & I_R \cdot \sin^2(\omega t + k x_R) \\ & - 2 A_R A_M \sin(\omega t + k x_R) \cdot \sin(\omega t + k x_M) \\ & + I_M \cdot \sin^2(\omega t + k x_M) \end{aligned}$$

If we use lasers with a red line as the light source, e.g. the Helium-Neon laser at a wavelength of 0.632 μm, the radian frequency will be $\omega = 2\pi\nu$ or the frequency ν:

$$\nu = \frac{c}{\lambda} = \frac{3 \cdot 10^8}{0.632 \cdot 10^{-6}} = 4.75 \cdot 10^{14}\ Hz$$

Except of course, the eye, there is to date, still no other detector that is even close to being this fast. Intensities which oscillate at that fast speed are therefore taken only as temporary mean values. The temporary mean value of $sin^2(\omega t)$ is $^1/_2$, therefore:

$$I_1 = I_R + I_M - 2\sqrt{I_R I_M}\, \sin(\omega t + k x_R)\sin(\omega t + k x_M)$$

If we use the theorem of addition

$$\frac{1}{2} \cdot \left(\cos(\alpha - \beta) - \cos(\alpha + \beta) \right) = \sin\alpha \cdot \sin\beta$$

and observe that the temporary average value of $cos(\omega t)=0$, the result would be:

$$I_1 = \frac{I_R + I_M}{2} - \sqrt{I_R I_M} \cdot \cos\delta \qquad \textbf{(1)}$$

$$\delta = k \cdot (x_R - x_M) = 2\pi \cdot \frac{(x_R - x_M)}{\lambda}$$

or with $I_R = I_M = {}^1/_2 I_0$ (beam split is exactly 50% / 50%)

$$I_1 = \frac{I_0}{2}(1 - \cos\delta)\ \text{for Exit 1} \qquad \textbf{(2)}$$

$$I_1 = \frac{I_0}{2}(1 + \cos\delta)\ \text{for Exit 2} \qquad \textbf{(3)}$$

If the path difference δ is zero, i.e. x_R - x_M = 0, then I_1 is equal to zero and I_2 is equal to I_0.

If the path difference δ is π i.e. x_R - x_M = $\lambda /2$, I_2 equals zero and I_1 equals I_0.

A shift of the measuring beam reflector of only $\lambda/4$ (0.000158 mm!) is sufficient for this to occur, since the measuring path is traversed twice.
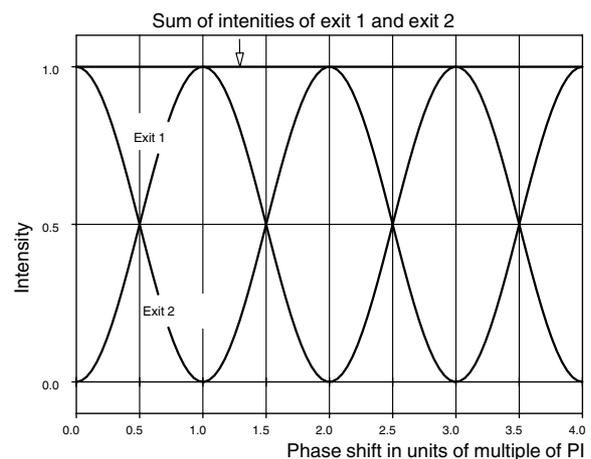
Fig. 6: Diagram of the Intensity I_1, I_2 and the sum of I_1 + I_2 as a function of the path difference δ

This function of the Michelson interferometer can normally not be found in textbooks and manuals. This is why the question: Where is the interferometer's energy in the case of destructive interference? is often raised. The answer is: every interferometer has at least two exits which naturally

must have a phase difference of 180°. The second exit of the Michelson interferometer as shown in Fig. 4 leads back to the light source. This line-up is, therefore, not of much use in techniques for laser measurement, since the light is completely reflected back into the laser in one particular path difference and thus destroys the oscillation mode of the laser. It is for this reason that the modification of the Michelson interferometer as shown in Fig. 4 is used in such cases.

1.2 Real interferometers

If the beam splitter ratio of division does not correspond exactly to 1, then the transmission curve changes according to Eq. 1 as shown in Fig. 7.
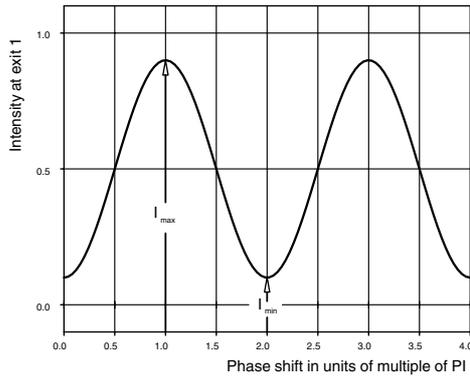
Fig. 7: Signal at Exit 1 at $I_R = 0.2\ I_0$ and $I_M = 0.8\ I_0$

At this point it would be appropriate to introduce the term V (Visibility), used to show contrast:

$$V = \frac{I_{max} - I_{min}}{I_{max} + I_{min}} \qquad (4)$$

according to equation (1) the result is:

$$I_{max} = \frac{1}{2}\left(I_R + I_M\right) + \sqrt{I_R \cdot I_M}$$

and

$$I_{min} = \frac{1}{2}\left(I_R + I_M\right) - \sqrt{I_R \cdot I_M}$$

or:

$$V = \frac{2 \cdot \sqrt{I_R \cdot I_M}}{I_R + I_M} \qquad (5)$$

In Fig. 6 the contrast V = 1 and in Fig. 7 V = 0.8.
A reduction in contrast can occur when, for example, the adjustment condition is not optimal. i.e. there is not a 100% overlapping of the beams I_M and I_R. The following then happens:

$$I_M + I_R < I_0 \qquad \text{see Fig. 8}$$
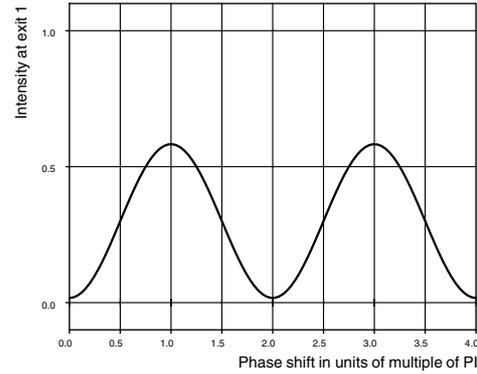
Fig. 8: **The interference signal given at Exit 1 at $I_M = 0.2\ I_0$ and $I_R = 0.4\ I_0$, is caused by maladjustment and not by an ideal beam splitter**

Till now we have tacitly assumed that the source of light only has a sharp frequency of ω.In practice this is never the case. Even lasers have a final emission band width δω,limiting the length of coherence L_c to:

$$L_c = \frac{c}{\delta\nu} \qquad (6)$$
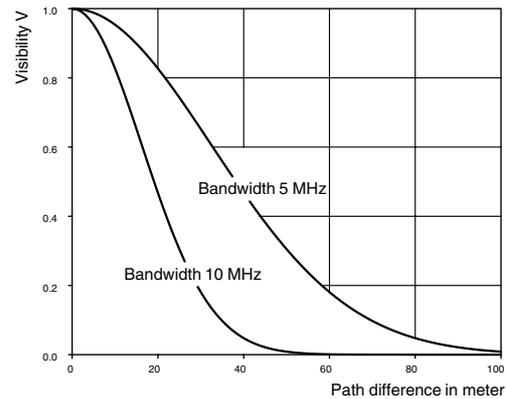
Fig. 9: **Contrast as a function of the path difference of a light source with an emission bandwidth of 5 and 10 MHz (Laser)**

Although the interferometer is ideal, the contrast obtained will not be good if the emission bandwidth of the light source is wide. Michelson carried out his experiments with the red line of a cadmium lamp which had a coherence length of only 20 cm. Since the index arm is traversed twice the measurement area available for him to work on was only 10 cm.
Since a two mode laser emits two distinct frequencies, even though this is done within a narrow bandwidth, the contrast function shows zero setting in the distance between the modes.
The line width of the light source can be deduced with Eq. 6 by measuring the contrast function. We should bear in mind that Michelson carried this out on the green Hg-line and captured 540,000 wavelengths of path difference with the naked eye in the process, Perot and Fabry brought the figure up to 790,000 and Gehrcke made it as far as 2,600,000 !
Imagine this: Shifting the measurement reflector, observing the light/dark stripes with the eye and counting to 2,600,000 at the same time.
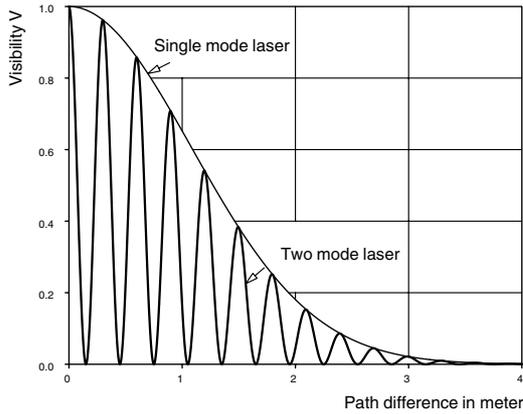
Fig. 10: **Contrast as a function of the path difference of a mono mode and a two mode laser**

It is no wonder then, that people were concerned about making a better device that could achieve the goal, i.e. measuring line widths in a way that would take less time.

This finally lead to the development of Fabry and Perot's multibeam interferometer, which will be discussed in the next chapter.

All the basic characteristics of the two-beam interferometer mentioned discussed in the last chapter also apply to the multibeam interferometer, and in particular, to the formulae required for calculating the interference terms.

2 Multibeam interferometer

2.1 The Ideal Fabry Perot
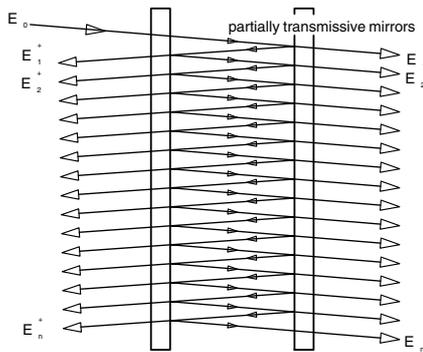
Fig. 11: **Fabry and Perot's multibeam interferometer**

The two plates are at a distance d from each other and have a reflectivity R. Absorption should be ignored, resulting in R = 1-T (T = Transmission). The wave falls under the angle α in the Fabry Perot (from now onwards referred to as FP).

At this point we are only interested in the amplitudes A_i and will consider the sine term later (Fig. 12)
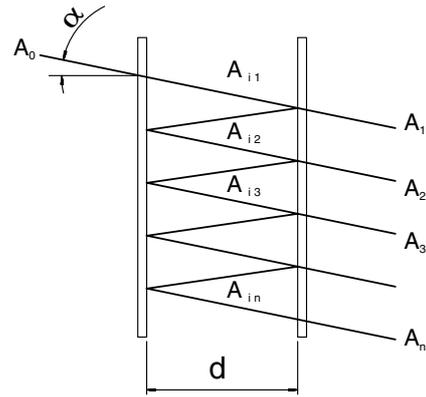
Fig. 12: Diagram of the derivation of the individual amplitudes

The incoming wave has the amplitude A_0 and the intensity I_0. After penetrating the first plate the intensity is

$$I_1 = (1 - R) \cdot I_0 = T \cdot I_0$$

since $\qquad I = E^2$

we have $\qquad A_{i1} = \sqrt{1 - R} \cdot A_0$

$$A_{i2} = R \cdot A_{i1} = \sqrt{1 - R} \cdot R^1 \cdot A_0$$

$$A_{i3} = R \cdot A_{i2} = \sqrt{1 - R} \cdot R^2 \cdot A_0$$

$$A_{i4} = R \cdot A_{i3} = \sqrt{1 - R} \cdot R^3 \cdot A_0$$

$$A_{in} = R \cdot A_{i(n-1)} = \sqrt{1 - R} \cdot R^{n-1} \cdot A_0$$

The amplitudes A coming out of the second plate have the values:

$$A_1 = \sqrt{1 - R} \cdot A_{i1} = (1 - R) \cdot A_0$$

$$A_2 = \sqrt{1 - R} \cdot A_{i2} = (1 - R) \cdot R^2 A_0$$

$$A_3 = \sqrt{1 - R} \cdot A_{i3} = (1 - R) \cdot R^3 A_0$$

$$A_n = \sqrt{1 - R} \cdot A_{in} = (1 - R) \cdot R^n A_0$$

Now let us observe how much oscillation there is. Here, the following calculation can be made simpler if we use cos instead of sine.

$$E = A \cdot \cos(\omega t + kx + \delta)$$

δ is the phase shift with reference to E_1 It is created by passing through many long paths in the FP.

$$\delta = \frac{2kd}{\cos \alpha}$$

$$E_1 = A_1 \cdot \cos(\omega t + kx)$$

$$E_2 = A_2 \cdot \cos(\omega t + kx + \delta)$$

$$E_3 = A_3 \cdot \cos(\omega t + kx + 2 \cdot \delta)$$

$$E_n = A_n \cdot \cos(\omega t + kx + (n-1) \cdot \delta)$$

$$E_n = (1-R) \cdot R^n \cdot A_0 \cdot \cos(\omega t + kx + (n-1) \cdot \delta)$$

Just as with the two-beam interferometer the individual field intensities now have to be added up and then squared to obtain the intensity.

$$E = \sum_0^\infty E_n$$

To make further derivation easier, we will use the following equation:

$$\cos\gamma = \text{Re}[\cos\gamma - i \cdot \sin\gamma]$$

Re[ ] is the real component of a complex number.
With

$$\cos\gamma = \frac{e^{i\gamma} + e^{-i\gamma}}{2} \text{ and } \sin\gamma = \frac{e^{i\gamma} - e^{-i\gamma}}{2i}$$

$$\text{is } \cos\gamma = \text{Re}[e^{i\gamma}]$$

Due to the change in writing with complex numbers the rule for calculating intensity from a field intensity now is:

$$I = E \cdot E^*$$

in which case E^* is the conjugate-complex of E (Rule: exchange i with -i). The following sum of individual field intensities must now be calculated:

$$E = \text{Re}\left\{ e^{i(\omega t + kx)} \cdot \sum_{n=1}^p A_n \cdot e^{i(n-1)\delta} \right\}$$

Inserted for A_n and $e^{-i\delta}$ from the sum of *n= 1* till *p* reflections taken out:

$$E = \text{Re}\left\{ e^{i(\omega t + kx)} \cdot (1-R) \cdot A_0 \cdot \sum_{n=1}^p R^n \cdot e^{i(n-1)\delta} \right\}$$

$$E = \text{Re}\left\{ e^{i(\omega t + kx)} \cdot (1-R) \cdot A_0 \cdot e^{-i\delta} \cdot \sum_{n=1}^p R^n \cdot e^{in\delta} \right\}$$

The sum shows a geometric series, the result of which is:

$$\sum_{n=1}^p R^n \cdot e^{in\delta} = \frac{1 - R^p \cdot e^{ip\delta}}{1 - R \cdot e^{i\delta}}$$

For the electric field strength E we get:

$$E = \text{Re}\left\{ e^{i(\omega t + kx)} \cdot (1-R) \cdot A_0 \cdot e^{-i\delta} \cdot \frac{1 - \cdot R^p \cdot e^{ip\delta}}{1 - R \cdot e^{i\delta}} \right\}$$

If we now increase the reflections p to an infinite number, R^p will go against zero since R<1 and the result is:

$$E = \text{Re}\left\{ e^{i(\omega t + kx)} \cdot (1-R) \cdot A_0 \cdot e^{-i\delta} \cdot \frac{1}{1 - R \cdot e^{i\delta}} \right\}$$

The intensity is established by:

$$I = E \cdot E^*$$

$$I = I_0 \frac{(1-R)^2}{(1 - R \cdot e^{i\delta}) \cdot (1 - R \cdot e^{-i\delta})}$$

$$I = I_0 \frac{(1-R)^2}{1 - R \cdot e^{i\delta} - \text{Re}^{-i\delta} + R^2}$$

$$I = I_0 \frac{(1-R)^2}{1 + R^2 - 2R\cos\delta}$$

$$\text{with} \quad 2 \cdot \sin^2\left(\frac{\delta}{2}\right) = 1 - \cos\delta$$

resulting in:

$$I = I_0 \frac{(1-R)^2}{1 + R^2 - 2R \cdot (1 - 2\sin^2(\delta/2))}$$

and finally:

$$I = I_0 \frac{(1-R)^2}{(1-R)^2 + 4 \cdot R \cdot \sin^2(\delta/2)}$$

Let us now add the abbreviation for δ again and observe that for an infinite number of reflections either the angle of incidence α becomes zero or the mirrors have to be infinitely large. If α is set equal to zero, then we get

$$\delta = \frac{2 \cdot d \cdot k}{\cos\alpha} = 2 \cdot d \cdot k$$

and the final result:

$$I = I_0 \frac{(1-R)^2}{(1-R)^2 + 4 \cdot R \cdot \sin^2\left(\frac{2\pi d}{\lambda}\right)} \qquad (7)$$

This function was first derived by G.B. Airy (Philos.Mag. (3) Bd.2 (1833)). It is shown in Fig. 13
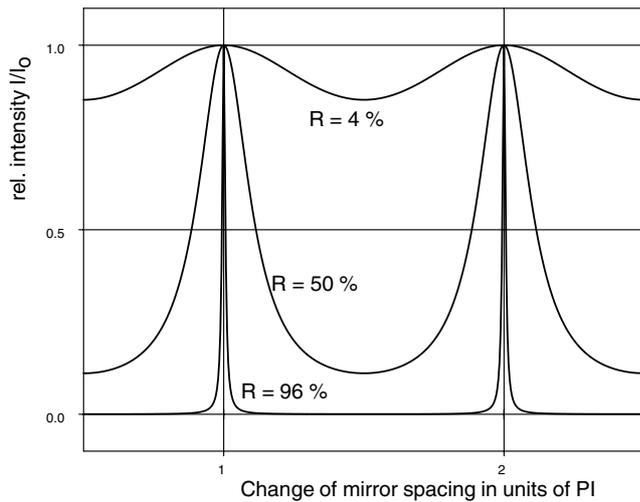
Fig. 13: **The transmission curves of a Fabry Perot interferometer (resonator) for different degrees of mirror reflection *R***

If the transmission curve for a reflection coefficient of .96 is compared to the transmission curve of a Michelson interferometer (Fig. 14) it can be seen that the Fabry Perot has a much sharper curve form.
This makes it easier to determine the certainty of the occurrence of a shift of λ/2.)
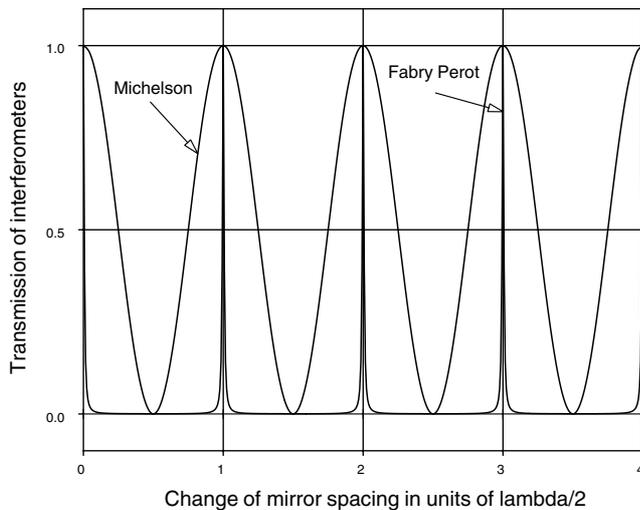
Fig. 14: **Comparison between the Michelson and the Fabry Perot Interferometers**

At first it seems astonishing that at the point of resonance where the mirror distances of the Fabry Perot are just about a multiple of half the wavelength, the transmission is 1, as if there were no mirrors there at all.

Let us take, for example, a simple helium-neon laser with 1 mW of power output as a light source and lead the laser beam into a Fabry Perot with mirror reflections of 96%.
The resonance obtained at the exit will also be 1 mW. This means that there has to be 24 mW of laser power in the interferometer because 4% is just about 1 mW. Magic? - no, not at all - This reveals the characteristics of the resonator in

the Fabry Perot interferometer. It is, in fact, capable of storing energy. The luminous power is situated between the mirrors. This is why the Fabry Perot is both an interferometer as well as a resonator. It becomes a resonator when the mirror distance is definitely adjusted to resonance, as is the case, for example, with lasers.
There are three areas of use for the Fabry Perot:

1. As a Length measuring equipment for a known wavelength of the light source. The Michelson interferometer offers better possibilities for this.

2. As a High-resolution spectrometer for measuring line intervals and line widths(optical spectrum analyser)

3. As a High quality optical resonator for the construction of lasers.

In the following series of experiments the Fabry Perot is used as a high-resolution spectrometer. Its special characteristics are tested and measured.

All the parameters required for an understanding of the Fabry Perot as a laser resonator are obtained in the process. At the end of the chapter on the fundamentals, the most important parameters of the FP will be discussed, using the ideal FP as an example first, so we can then discuss the practical aspects, which lead to the divergences from the ideal behaviour in the chapter on the real FP. Fig. 15 is shown to get an idea of the practical side in the introductory chapter itself.

We are looking at the spectrum analyser with the FP as shown in Fig. 15.
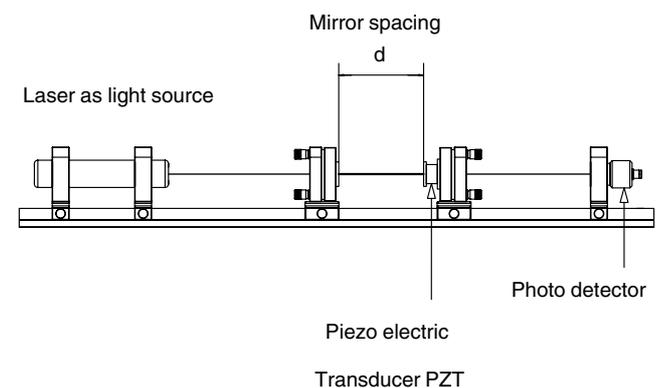
Fig. 15:Experimental situation

The FP is formed out of two mirrors, fixed parallel to each other by adjustment supports. A mirror is fixed on to a Piezo element.

This element allows the variation of a mirror distance of some μm by applying an electric voltage (Piezo element). The transmitted light of the FP is lead on to a photo detector. A monochromatic laser with a low band width is used as a light source. Linear changes in the mirror distance take

place periodically and the signal is shown on an oscilloscope (Fig. 16).
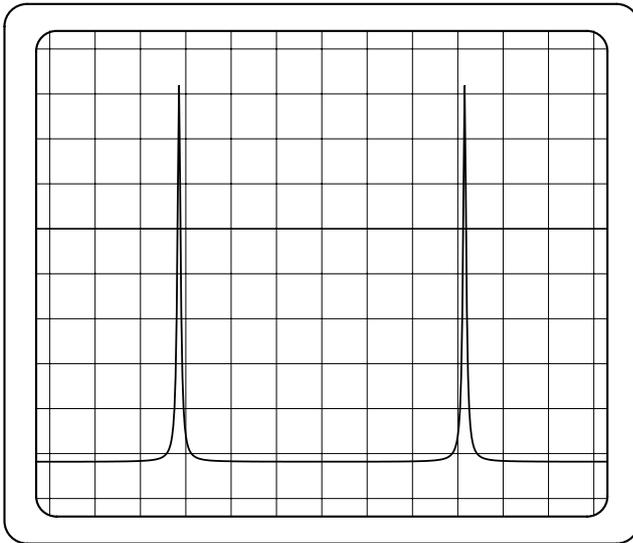
Fig. 16: Transmission signal on an oscilloscope with a periodic variation of the mirror distance d

The parameters of the FP will now be explained using this diagram. Two transmission signals can be seen. It is obvious that the distance d of the FP has been changed to a path just over $\lambda/2$. In our example we have used a He-Ne laser with the wavelength 632 nm, so the change in distance was just over 316 nm or 0.000316 mm. The distance between the peaks corresponds to a change in length of the resonator distance of exactly $\lambda/2$ according to Eq. (7). The distance between the two peaks is known as the:

Free Spectral Range FSR.

This range depends on the distance d of the mirrors as shown below. For practical reasons, this distance can be given in Hz. To calculate this we must ask ourselves: How much would the light frequency have to change for the FP to travel from one resonance to the next at the now fixed distance d ?

The light wave is reflected on the mirrors of the resonator and returns back to itself. The electric field intensity of the wave at the mirrors is therefore zero. At a given distance d the mirrors can only form waves which have the field intensity of zero at both mirrors. It is obviously possible for several waves to fit into the resonator if an integer multiple of half the wavelength is equal to d.

The waves, which fit into a resonator of a particular length are also called oscillating modes or just modes. If the integer is called n then all waves which fulfil the following equation will fit into the resonator:

$$d = n \cdot \frac{\lambda_1}{2}$$

The next neighbouring mode must fulfil the condition

$$d = (n+1) \cdot \frac{\lambda_2}{2}$$

The difference between the two equations above gives us:

$$n \cdot \frac{\lambda_1}{2} - (n+1) \cdot \frac{\lambda_2}{2} = 0$$

or

$$\lambda_1 - \lambda_2 = \frac{\lambda_2}{n} = \frac{\lambda_1 \cdot \lambda_2}{2 \cdot d}$$

$$\frac{\delta\lambda}{\lambda_1 \cdot \lambda_2} = \frac{1}{2 \cdot d}$$

and

$$\nu = \frac{c}{\lambda} \Rightarrow \delta\nu = c \cdot \frac{\delta\lambda}{\lambda_1 \cdot \lambda_2}$$

ν is the frequency of light and c the speed of light. The result for the free spectral range in use is:

$$\delta\nu = \frac{c}{2 \cdot d} \qquad\qquad (8)$$

The size $\delta\nu$ is also called the mode distance. In an FP with a length L 50 mm, for example, the free spectral range or mode distance is $\delta\nu = 3$ GHz.

We can also deduce, from the size of the free spectral range calculated above, that the FP in Fig. 15 was tuned to 3 GHz with the mirror distance at 50 mm. If we increase the distance of the FP mirror to 100 mm the size of the FSR between two resonance peaks is 1.5 GHz. Bearing in mind that the frequency of the He-Ne Laser (λ = 632 nm) is 4.75 10^5 GHz, a frequency change in the laser of at least $\Delta\nu/\nu = 3 \; 10^{-6}$ can be proved.
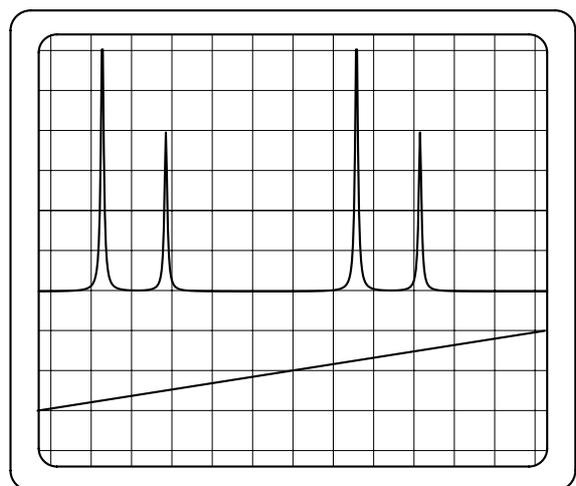
Fig. 17: Example of a scan of a two mode laser. The lower trace shows the change in length of the FP.

In the example shown in Fig. 17 the spectrum of a two mode laser was recorded. Two groups can be seen, consisting of two resonance peaks. Since the free spectral range,

i.e. the distance between two similar peaks is known (through the measurement of the mirror distance and equation 8) the distance between the frequencies of two neighbouring peaks is also known and their difference in frequency can be measured precisely. Measurement of the absolute frequency with a Fabry Perot is, however, only possible if the exact mirror distance d is known. But this would involve considerable practical difficulties, since the determination of the length measurement would have to be $< 10^{-6}$. At 50 mm this means $\delta d = \delta\lambda/\lambda\ 0.05\ m = 5\ 10^{-8}\ m = 50\ nm$!

A second important parameter of the Fabry Perot is its finesse or quality. This determines its resolution capacity. Fig. 13 shows the transmission curves for various reflection coefficients of the mirrors. There is clearly a connection between the width of a resonance peak and the value of reflection. It therefore makes sense to define the finesse as a quality:

$$F = \frac{FSR}{\Delta\nu}$$
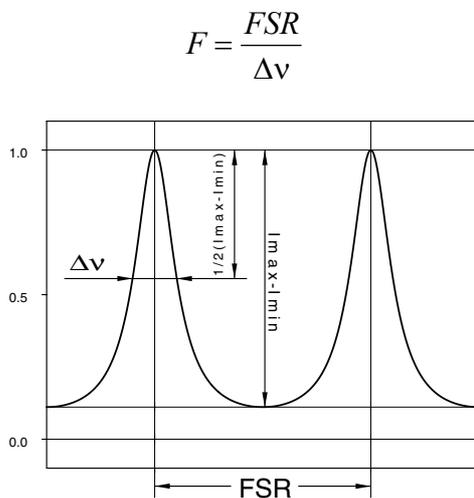
Fig. 18: Definition of finesse

For this purpose the full width at half maximum $\Delta\nu$ (FWHM) is calculated

$$I = \frac{I_{max} - I_{min}}{2}.$$

Let us assume that R≈1. Then $I_{min} \approx 0$ and

$$I = \frac{I_{max} - I_{min}}{2} \approx \frac{I_{max}}{2}$$

or $I / I_0 = \frac{1}{2}$. The values δ_1 and δ_2 can be calculated with Eq. 7 where the intensity is just about $\frac{1}{2} I_0$.

$$\frac{I}{I_0} = \frac{1}{2} = \frac{(1-R)^2}{(1-R)^2 + 4 \cdot R \cdot \sin^2\left(\frac{\delta}{2}\right)}$$

$$(1-R)^2 + 4 \cdot R \cdot \sin^2\left(\frac{\delta}{2}\right) = 2 \cdot (1-R)^2$$

$$4 \cdot R \cdot \sin^2\left(\frac{\delta}{2}\right) = (1-R)^2$$

$$\sin\left(\frac{\delta}{2}\right) = \pm\frac{1-R}{2 \cdot \sqrt{R}}$$

$$\delta_1 = 2 \cdot \arcsin\left(\frac{1-R}{2 \cdot \sqrt{R}}\right)$$

$$\delta_2 = -2 \cdot \arcsin\left(\frac{1-R}{2 \cdot \sqrt{R}}\right)$$

since (1 - R) << R, the function arcsin can be replaced by its argument:

$$\delta_1 - \delta_2 = 2 \cdot \frac{1-R}{\sqrt{R}}$$

with $\delta = k \cdot 2d = \frac{2\pi}{\lambda} \cdot 2d = \frac{2\pi\nu}{c} \cdot 2d$

$$\delta_1 - \delta_2 = \frac{4\pi d}{c} \cdot \Delta\nu = 2 \cdot \frac{1-R}{\sqrt{R}}$$

$$\Delta\nu = \frac{c}{2\pi d} \cdot \frac{1-R}{\sqrt{R}}$$

Due to the definition

$$F = \frac{FSR}{\Delta\nu}$$

we get by substituting for F:

$$F = \frac{c \cdot \sqrt{R} \cdot 2\pi \cdot d}{2d \cdot c \cdot (1-R)} = \frac{\pi\sqrt{R}}{1-R} \qquad \textbf{(9)}$$

As we have already assumed, the finesse depends on the reflectivity R of the mirrors. This is also shown in Fig. 13. The tendency now would be to bring the reflectivity R as close as possible to 1 to achieve a high finesse.

There are, however limitations in the finesse for the plane mirror of the Fabry Perot that has been discussed till now. These limitations lie in the imperfection of the mirror surfaces, which do not exist to a great extent in the spherical FP's yet to be discussed.
So, in the next chapter we intend to address these problems.

2.2 The real Fabry Perot

The finesse cannot be increased to over 50 even if a plane mirror of high technical precision is used. A finesse of 50 requires a plane of $\lambda/100$ (λ approx. 500 nm) i.e. around 0.000005 mm = 5 nm !

This is because in anything other than an ideal plane mirror surface, the beams do not reflect back precisely, but they diverge from the ideal path in approximately thousands of rotations. This blurs the clear phase relationship between the waves and as a consequence the resonance curve becomes wider.
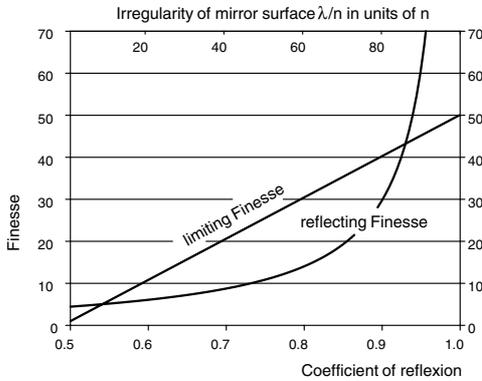
Fig. 19: Limitation of the finesse by the imperfect plane of the mirror surfaces in the plane Fabry Perot

If, on the other hand, spherical mirrors are used, then the occurrence of mistakes in sensitivity are much less. In the case of spherical FP's however, care must be taken that the diameter of the light falling in is smaller than the diameter of the mirrors. Generally speaking, this can be accomplished particularly well in laser applications. Plane FP's have thus very little significance in laser technology.

2.3 The Spherical Fabry Perot

A spherical Fabry Perot consists of two mirrors with a radius of curvature r. The most frequently used FP is the confocal FP where the mirror distance L is equal to r (Fig. 20). The path difference δ is 4r for beams close to the centre. So, the free spectral range FSR (δν) is:

$$\delta\nu = \frac{c}{4\cdot d} \qquad (\,10\,)$$

But the spherical FP is not subjected to the limitations of a plane mirror in terms of total finesse based on divergences from the ideal mirror surface or maladjustment. If the mirror of a plane FP is turned over ε, a beam scanning of 2ε is brought about. Due to the imaging characteristic of spherical mirrors, maladjustment has a much lesser effect on the total finesse. The limiting finesse of a spherical FP is therefore mainly the reflection finesse. Moreover, spherical mirrors can be produced more precisely than plane mirrors.
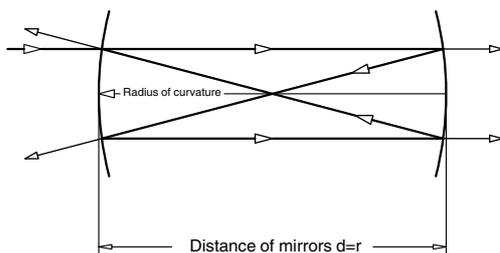
Fig. 20: Confocal Fabry Perot
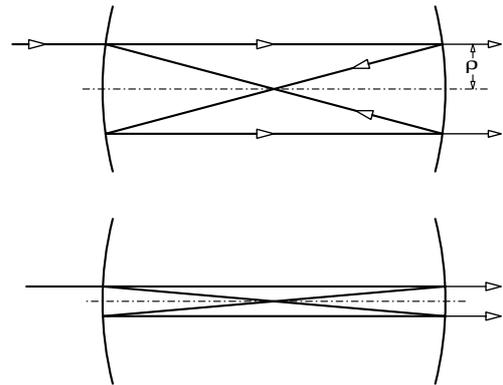
Fig. 21: Confocal FP at various beam radii ρ

2.4 The Spherical FP in practice

The first mirror of the FP has the effect of a plane-concave lens. The incoming beam is therefore scanned as shown in Fig. 22. A biconvex lens enables the incoming beam to run parallel to the optical axis within the FP.
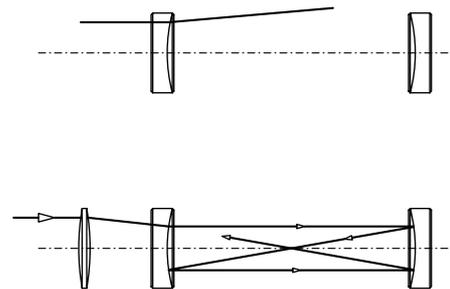
Fig. 22: A biconvex lens is required to make the incoming beam run parallel to the optical axis
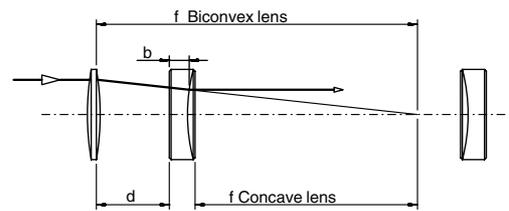
Fig. 23: Course travelled by the beam for the calculation of the focal distance and position of the biconvex lens.

The above mentioned is also true for the beam exit and a lens is put in front of the photo detector for this purpose. Other effects can also be achieved with this lens. If the condition ρ<<R cannot be executed, there is a dislocation of the point of intersection of the interfering beams in the resonator [2], due to spherical aberrations of the mirrors. If this plane of intersection is imaged with a lens, the finesse will still be good.

Another important point is the exact distance between the mirrors. In a spherical FP, for example r=100 mm, the error should not be more than 14 μm. The distance between the mirrors is varied by a few millimetres to find this point. The oscilloscope shows the image in Fig. 24.
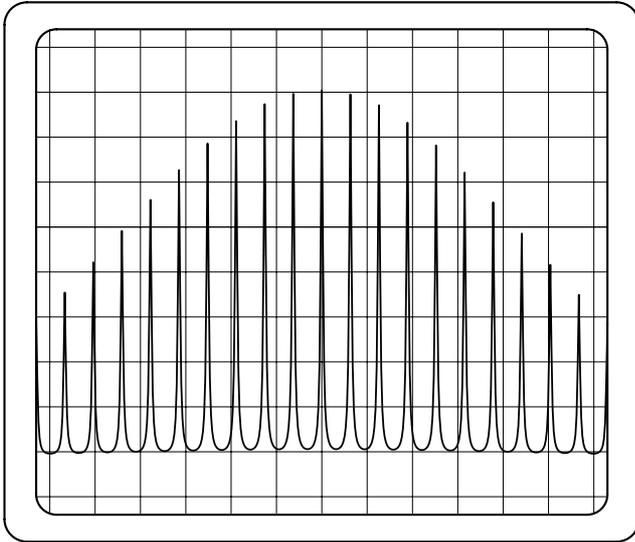
Fig. 24: **The contrast is more intense close to d = r. At d ≡ r the confocal case has been reached and the contrast is at its maximum.**

Apart from the confocal FP, other types of spherical resonators can be devised. As a necessary prerequisite, they must fulfil the criteria for stability.

$$0 \le g_1 \cdot g_2 \le 1$$

$$g_i = 1 - \frac{d}{r_i}.$$

d is the mirror distance and r the mirror radius. The Index i is for the left mirror l or for the right mirror 2. If the product $g_1 g_2$ sufficiently fulfils the above condition, the resonator is optically stable (Fig. 25).

Various combinations can be executed in the shaded areas as far as the radius of curvature r and the mirror distance d are concerned. Both have a more or less good finesse, representing an important parameter for the FP as a spectrum analyser.

The highest finesse is achieved with a confocal resonator (B). Here d = r and g_1 and g_2 are zero.

The plane FP has g-values of 1 since r is infinite (A). Finally we can choose a concentric arrangement with a mirror distance of d = 2r and g-values of -1. This case has been marked by C.
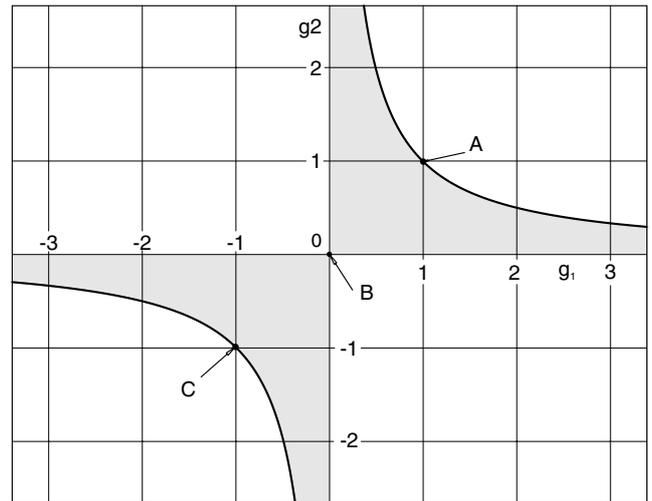
Fig. 25: Stability of optical resonators

3 Bibliography

[1] Wulfhard Lange

Introduction to laser physics
Wissenschaftliche Buchgesellschaft Darmstadt Germany
ISBN 3-534-06835-1

[2] 2 W. Demtröder

Basics and techniques of laser spectroscopy
Springer-Verlag Germany
ISBN 3-540-08331-6

4 Experimental set-up
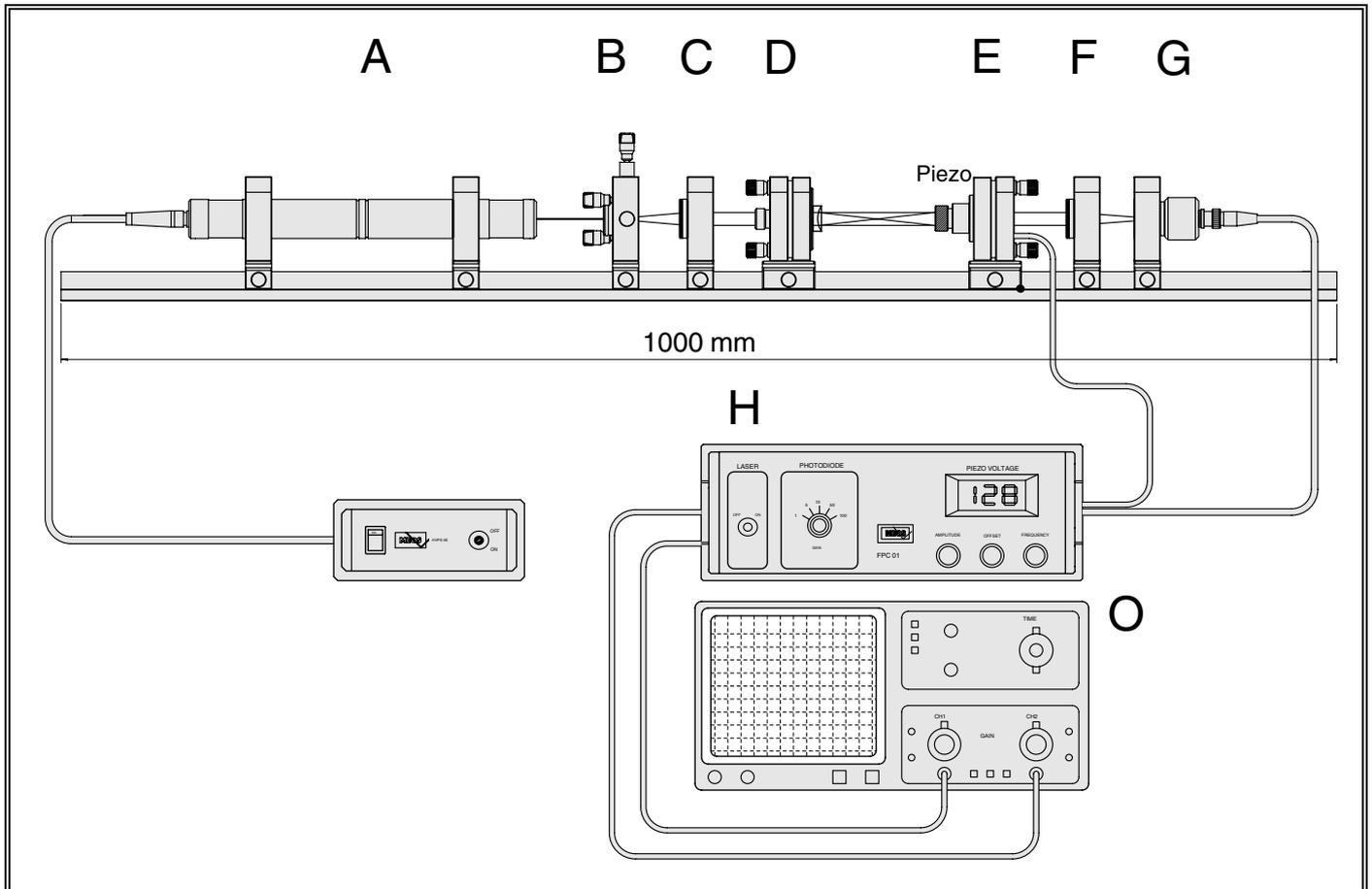
The experimental set-up consists of two mirror adjustment supports (module D and E)in which the mirrors of the Fabry Perot resonator are accommodated. One mirror is attached to a Piezo element (module E) which produces linear expansion, periodically. Both mirrors can be easily interchanged. The mirror adjustment support with the Piezo element is attached to a linear displacement mechanism to achieve confocal adjustment. The spectrum of the He-Ne laser beam to be taken up, is adjusted to the required beam radius as well as divergence, using a telescope (module B and C). A collimating lens is positioned before the photo detector (module G) to ensure optimum illuminating in each case. The photo detector is connected by means of a BNC cable to the rear of the controller (module H). The gain selector of the built-in photodiode amplifier is placed on the front panel. Its output is on the rear of the controller. BNC plugs/sockets & cables are used to make the necessary connections. A periodic linear change in the Piezo voltage can occur at a range of 0-150 V. The frequency is tuned with the appropriate regulator on the front panel of the apparatus to obtain an image on the oscilloscope that does not flicker. There is a low voltage output at the rear, which when connected to the oscilloscope shows the Piezo swing. The amplitude and with it, the number of sequences passed through per cycle are tuned with an amplitude regulator. The spectrum can also be shifted with an Offset regulator.

4.1 Components

The optical rail, 1 m in length, on which the individual components are placed is not shown.
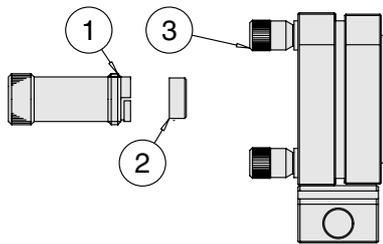
Module D

This module is the first part of the Fabry Perot resonator. The mirrors are mounted in holders (1) which are screwed into the laser mirror adjustment holder (3). All three mirrors (2) have a transmission of 4% for 632 nm. The radii of curvature are 75 mm, 100 mm and infinite.
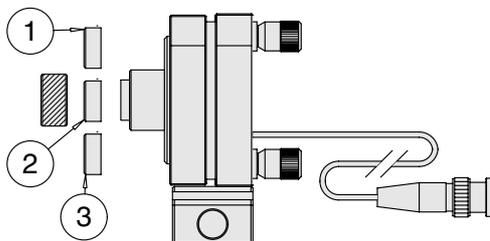
Module E

This is the second part of the Fabry Perot resonator. A Piezo-crystal is built into the laser mirror adjustment holder which has a threading at its front side. The individual mirrors (1,2,3) are mounted by means of a screw cap which has a soft O-ring at its inside. All three mirrors have a transmission of 4% for 632 nm. The radii of curvature are 75 mm, 100 mm and infinite. The carrier has a pinion driving screw and a gear rack which is inserted into the slot of the profile rail. So sensitive linear displacement variations of this laser mirror holder can be performed.
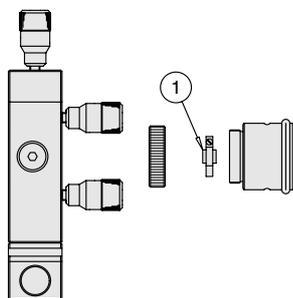
Module B

A lens (1) with short focal distance (f=5 mm) is the first component of the beam enlarging system which actually is made up of module B and module C. For the directional adjustment with regard to the optical axis this lens is mounted in a holder which can be adjusted in the XY-direction as well as in two orthogonal angles
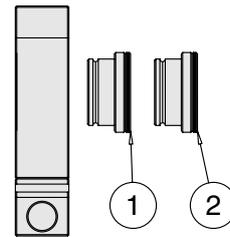
Module C

The module C has two parts to play. In connection with module B it forms the second part (f= 20 mm) of the beam enlarging system. The beam enlarging system is only of interest when plane parallel mirrors are used. At the use of spherical mirrors a lens (2) of f= 150 mm is inserted to compensate for the beam broadening of the plane concave mirror.
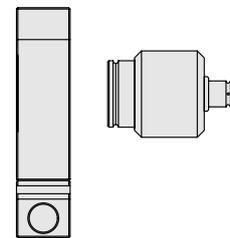
Module G

A PIN-photodiode mounted in a housing with „click"-mechanism and BNC-socket detects the interference pattern. The photodetector is „clicked" into the mounting plate on carrier. The inner pin of the BNC-socket is connected to the anode. By means of the attached BNC-cable the detector is connected to the amplifier of module H.
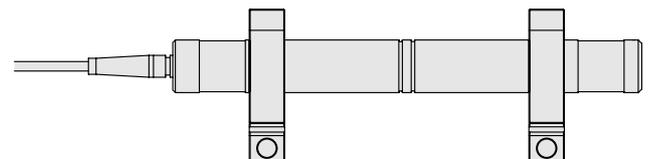
Module A

A HeNe-Laser is used as test laser. The emission spectrum consists of two longitudinal modes with a frequency distance of about 900 MHz. The modes are orthogonally polarised and linear. Two mounting plates with carrier are part of the module as well as the supply unit of the laser.
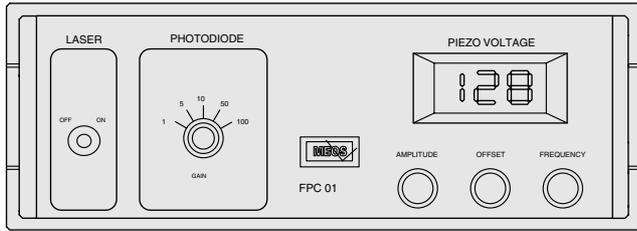
Module H

All voltages necessary for the supply of the Piezo-crystal and all monitor signals are generated by the controller FPC-01. It also contains the photodiode amplifier. The illustration at the right side shows the possibilities of voltage adjustment for the Piezo-crystal. The maximum voltage is 150 V. The frequency of the incorporated modulator for triangular signals can be adjusted up to 100 Hz. A monitor signal which is proportional to the selected Piezo-voltage is disposed by a BNC-socket at the rear. This signal should always be on the oscilloscope together with the photodetector signal to ensure that the Piezo-crystal is controlled correctly. The amplification of the built-in photodiode amplifier can be switched in five steps from 1 to 100. The control button is on the front panel of the unit.
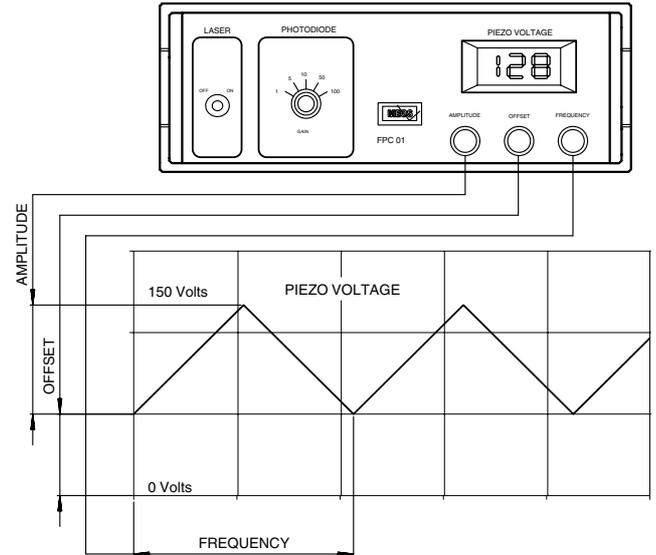
5 Experiments

5.1 Adjustment
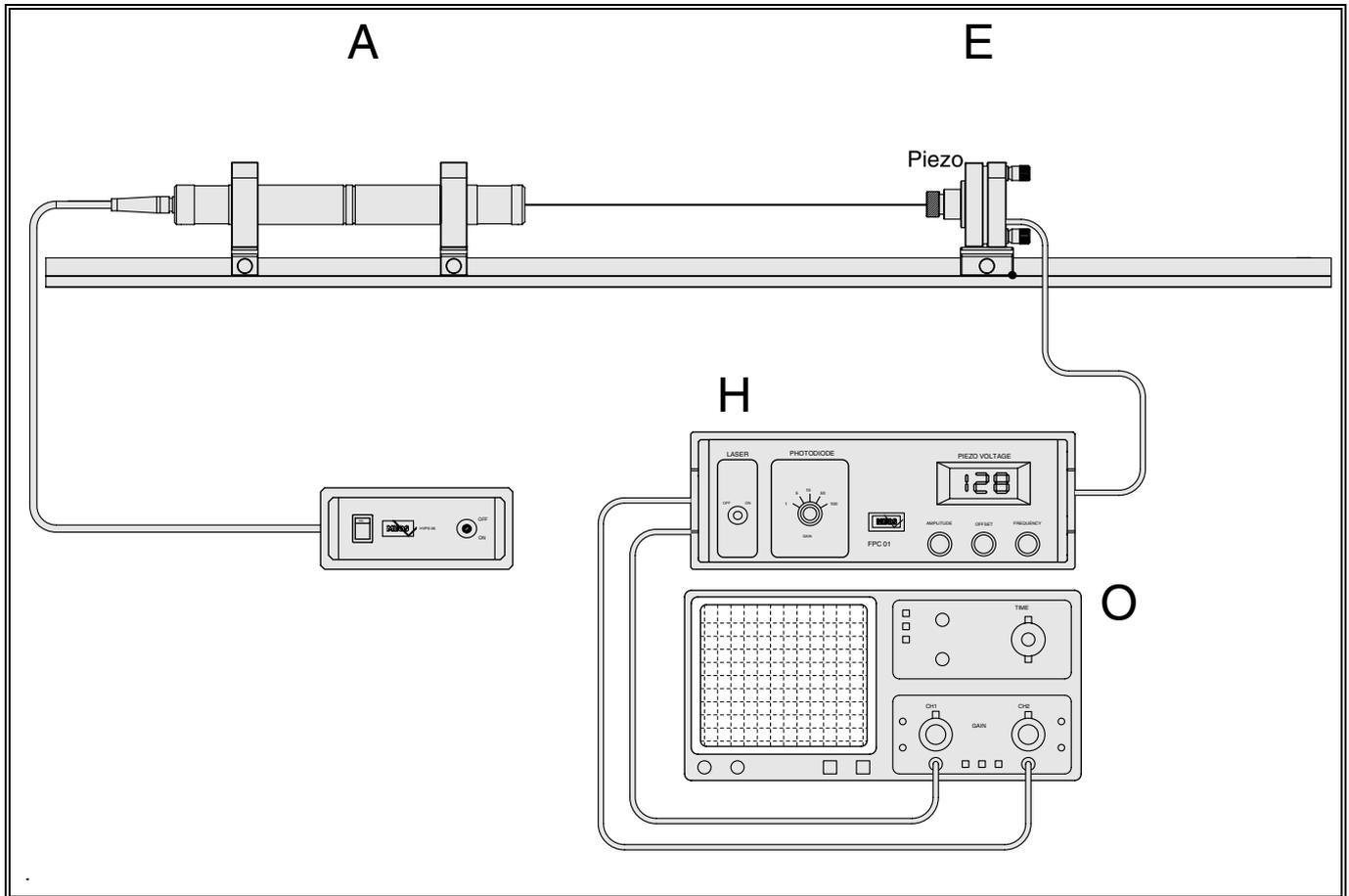
1. The components shown above are placed on to the rail and clicked into place. Use of a set of spherical mirrors is recommended for the first adjustment

2. The mirror adjustment holder "on the right hand side", is adjusted so that the beam going back, runs centred towards the laser beam. Due to the imaging characteristic of a spherical mirror the returning beam is expanded.

3. The Piezo voltage is tuned to maximum amplitude with the offset regulator to create a triangular voltage on the oscilloscope as shown in Fig. 26
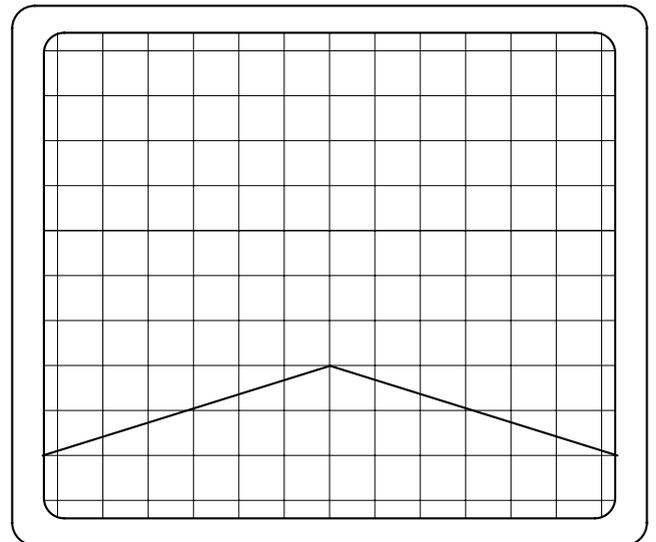
Fig. 26: The tuned in Piezo voltage should not be clipped, either at the top or at the bottom
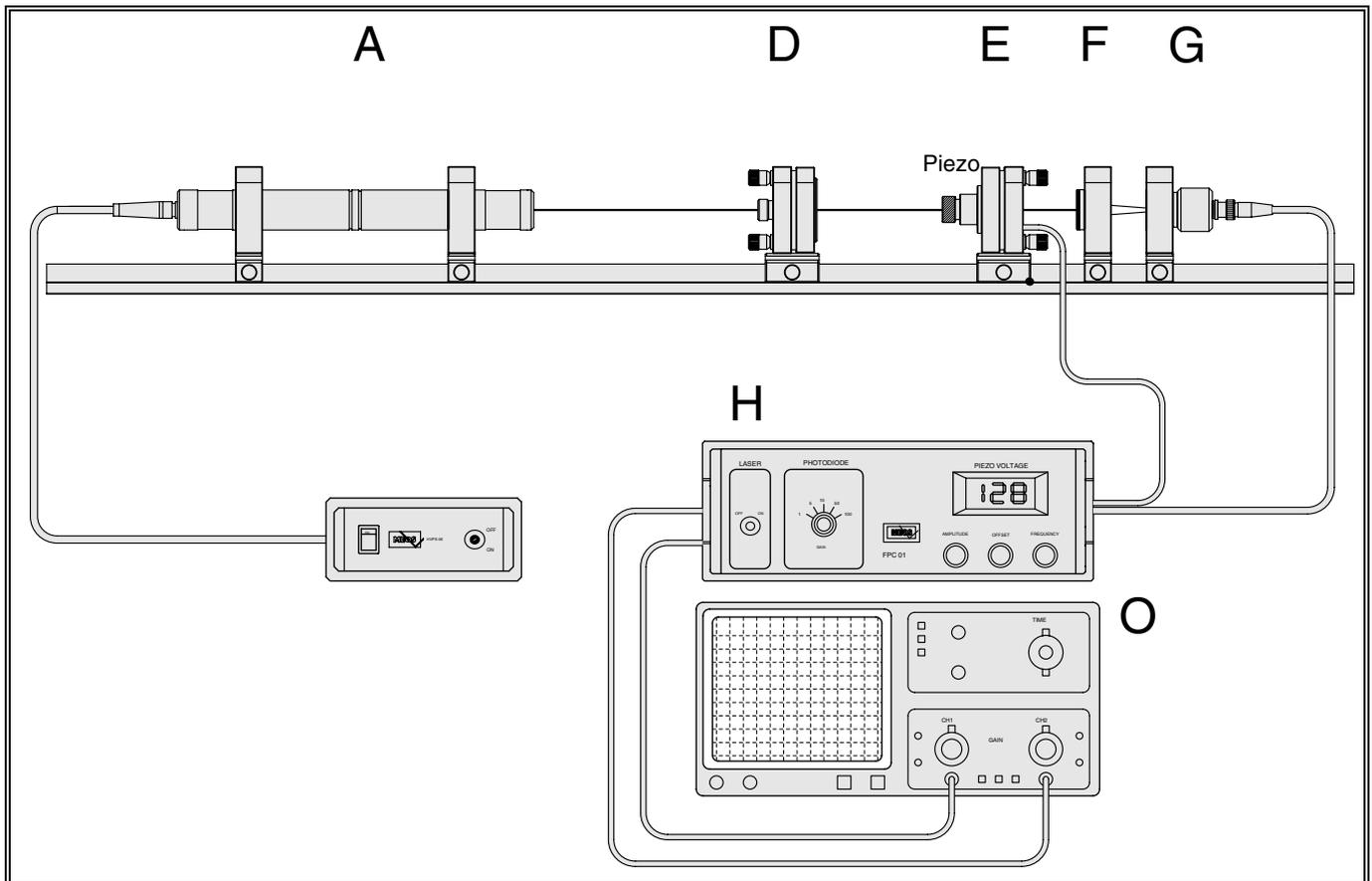
1. In the second step, the biconvex lens and the mirror adjustment holder are placed "on the left hand side". The mirror distance is chosen in such a way that d = r. The mirror placed into the adjustment support is then pre-adjusted and the returning beam will be centred towards the laser beam. Turn on the photo amplifier and adjust the oscilloscope to the maximum level of sensitivity and mode A/C.

Apart from the vibrations you will see the first "resonance humps". Keep adjusting the mirrors, making the "humps" increasingly clearer. You will have to continuously reduce the intensity simultaneously. When you have reached an optimum, you can shift the biconvex lens for maximum amplitude.

2. In the last adjustment step, the slide of the mirror adjustment support is gently released from the rail, "on the right hand side" and the distance d is changed with a line adjustment device. You can see the spectrum as shown in Fig. 27 coming close to the confocal case while the mirror adjustment support is being moved.

3. Repeat the individual adjustment steps till you have tuned in to a spectrum with the highest possible finesse. Optimise the convergent lens that is in front of the photo detector.
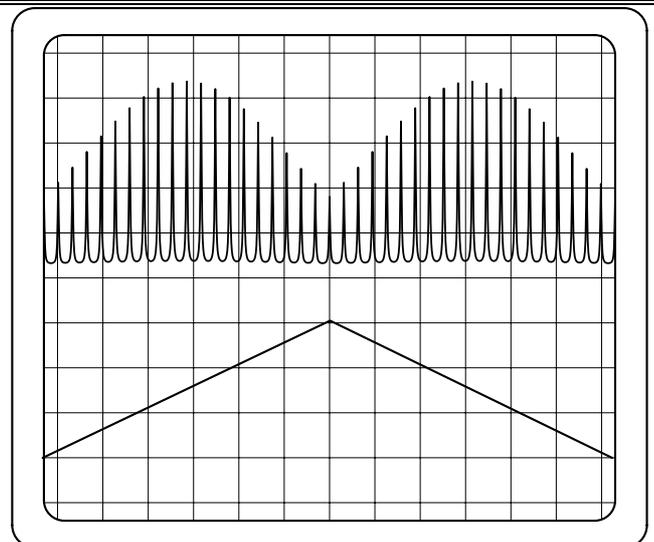
Fig. 27: Spectrum during the movement of the mirror support „on the right hand side" close to the confocal adjustment

5.2 Measurement of the FSR
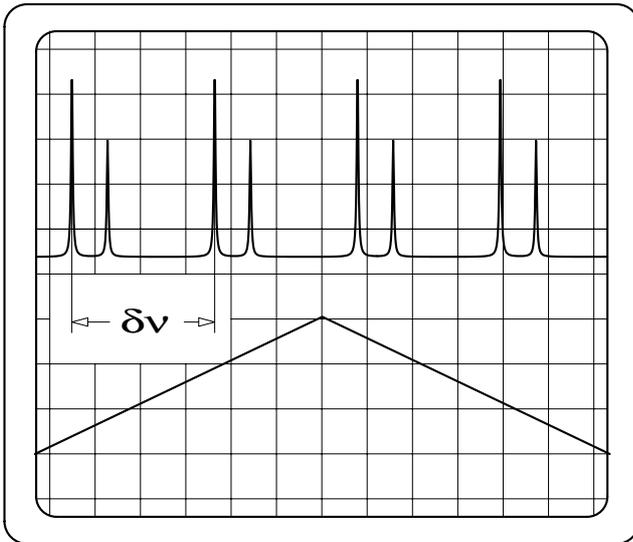
Fig. 28: Measurement of the free spectral range

1. If the adjustment has been made to the highest possible finesse, the free spectral range is determined in the next step (Eq. 8).
To do this, the amplitude has to be tuned down till only two sequences are left within the increase and decrease of the Piezo movement (Fig. 28).
2. The image can be made symmetrical with the offset adjustment. Using Eq. 8, the X axis of the oscilloscope can be calibrated in MHz light frequency (relative).
3. Since the path difference δ for the occurrence of two neighbouring resonance points according to Eq. 7, and the wavelength of the test laser (0.632 μm) are known, the specific expansion (μm /100 Volt) of the Piezo element can now be determined.

5.3 Measurement of the finesse
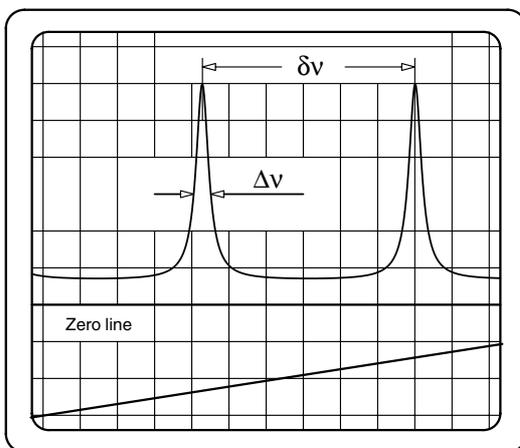
5.5 The plane Fabry Perot

1. For this measurement the electronic adjustments are selected in such a way that only two sequences fill the screen.
2. The photo detector's channel has to be set to DC for this measurement to obtain the base line for I_0.
3. The free spectral range for the calibration of the represented units on the oscilloscope is determined by the distance between two neighbouring sequences.
4. It is recommended to optimise the adjustments once more in this presentation.

5.4 Measurement of a mode spectrum
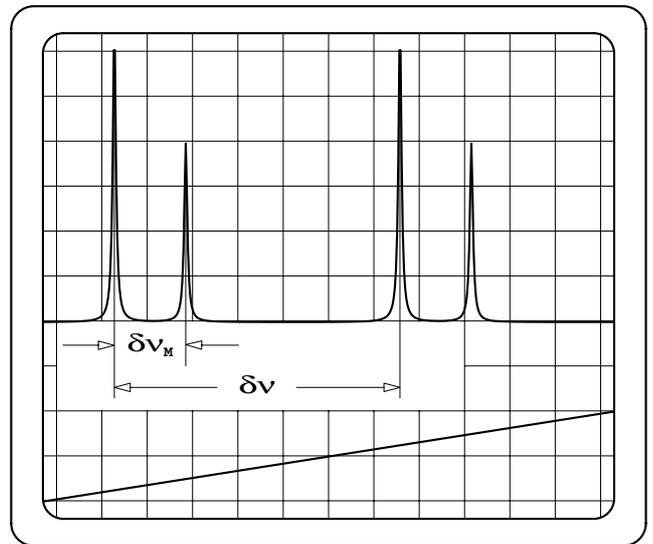
Fig. 30: Measurement of the mode distance $\delta\nu_M$ of the test laser

1. To measure the mode distance of the test laser, an example as shown in Fig. 30 should be selected. Once again the distance between two neighbouring sequences determines the frequency calibration and $\delta\nu_M$ can then be measured in units of frequency.

2. After completing this measurement you can switch off the test laser and allow it to cool for 2-3 minutes. When you switch it on again, the modes will now "pass across" the screen and you can observe the thermal running-in of the modes.

3. It is also possible to examine the polarising ability of the modes with a simple polarizer. If the laser does not have any built-in devices for polarisation selection (e.g. Brewster window), then the modes are polarised in different ways. The polarizer should be positioned directly behind the laser. By turning it, the disappearance of one mode or the other can be observed on the screen.
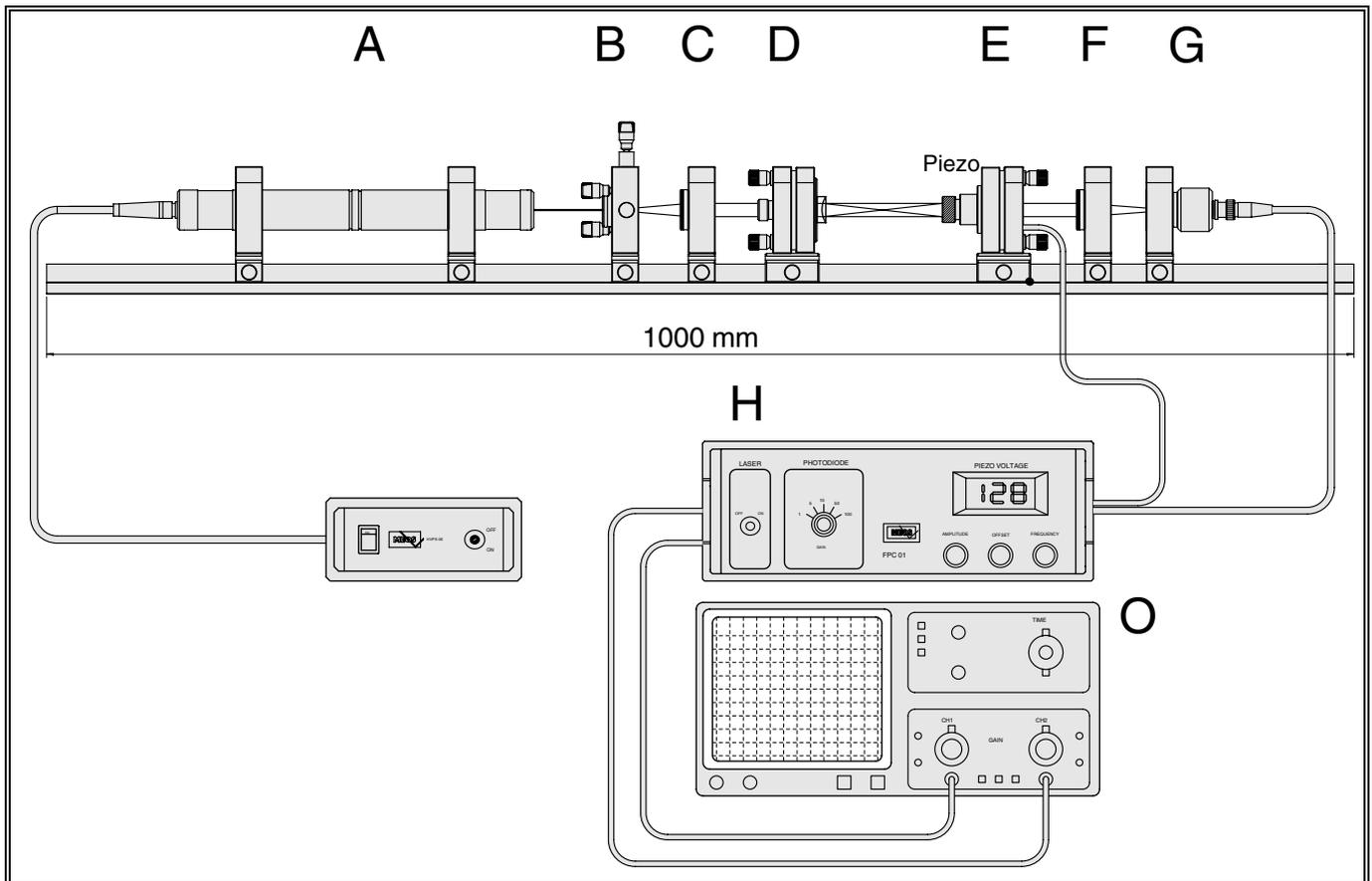
Fig. 31 Fabry Perot with plan mirrors and beam expanding telescope

1. The aim of this experiment is to clarify the difference between the plane FP and the spherical FP. The light of the test laser is first lead into the resonator, now equipped with plane mirrors, without `prior optical treatment'. The adjustment procedure is the same as for the spherical FP.

2. You will now see that the adjustment here is obviously more critical than in the case of a spherical FP.

3. Adjust the returning beam in such a way that it just misses returning into the test laser. Otherwise the FP acts as a resonator that is connected to the test laser resonator and the modes begin to oscillate irregularly.

4. The same measurements are carried out as in the spherical FP's.

5. Moreover, the beam can be expanded with the telescope, having a lens of =-5 mm and the achromatic lens f = 20 mm. Contrary to the spherical FP's, an increase in the finesse will be observed.